3D refractive index tomography with quantitative oblique back-illumination microscopy

Ledwig, Patrick, Robles, Francisco

Patrick B. Ledwig, Francisco E. Robles, "3D refractive index tomography with quantitative oblique back-illumination microscopy," Proc. SPIE 11245, Three-Dimensional and Multidimensional Microscopy: Image Acquisition and Processing XXVII, 1124503 (17 February 2020); doi: 10.1117/12.2544328

SPIE.

Event: SPIE BiOS, 2020, San Francisco, California, United States

3D refractive index tomography with quantitative oblique back-illumination microscopy

Patrick B. Ledwig[a] and Francisco E. Robles[a]

[a]Georgia Institute of Technology & Emory Univ. School of Medicine, Atlanta, Georgia, USA

ABSTRACT

We have recently developed quantitative oblique back-illumination microscopy (qOBM), which enables full-field quantitative phase imaging (QPI) of objects embedded in a thick scattering medium. This epi-mode technique makes use of multiple scattering as a source of transmissive illumination from within, allowing for rich structural detail based on optical path delay. We now produce quantitative 3D renderings of index of refraction with sub-cellular detail by computing a 3D transfer function of the entire optical system, including the multiply scattered illumination, and deconvolving it from a vertical stack of phase gradient contrast images. This approach allows truly non-invasive, label-free, tomographic quantitative reconstructions if index of refraction in thick scattering samples including thick tissue samples, at low cost and with simple operation, bringing QPI's unparalleled access to sub-cellular structural detail to previously unavailable domains of investigation.

Keywords: back illumination, quantitative phase, thick sample, refractive index, multiple scattering, differential phase contrast, microscopy, deconvolution

1. INTRODUCTION

Quantitative phase imaging is a label-free microscopy technique that uses contrast produced by variations in index of refraction within a thin sample to produce maps of phase delay encountered by incident light.[1] These maps provide valuable biomedical information from cells and tissues such as dry mass, sample thickness, and mass transport. Conventional QPI methods involve interfering beams from coherent sources, but phase-contrast images can be achieved with partially coherent sources.[2] Recently, it was shown that the phase maps produced from systems with partially coherent illumination arising from asymmetric illumination patterns, such as differential interference contrast (DIC),[3] and differential phase contrast (DPC),[4] can be quantified as readily as those produced by interferometric means, but without speckle noise or the need for expensive laser sources. This approach, in brief, works by producing an optical transfer function for the imaging system and then deconvolving it from the images gathered to produce the complex transmission function of the object.

While the 2D quantitative maps of phase produced by QPI provide valuable *in vitro* information about thin slices of histology or single cells, it only provides information regarding integrated optical path length. Therefore, in order to produce maps of refractive index, it is necessary in principle to acquire depth information through tomography. Three-dimensional maps of index of refraction can be produced with the conventional interferometric QPI approach with tomographic phase microscopy (TPM),[5] whereby a transparent, thin sample, such as a single cell, is illuminated from multiple angles, and the resultant distribution is reconstructed using methods analogous to those used in 3D medical imaging, such as filtered back-projection or beam propagation. More sophisticated reconstruction methods are a field of active research, but these methods typically require heavy computational resources and a limited field of view (e.g. a single cell).[6]

With partially-coherent phase contrast, the incoherence of the incident field produces an optical point spread function (PSF) with a limited axial extent, providing for inherent depth sectioning. Therefore, 3D images may be produced simply capturing a transverse through-stack of wide-field images. In principle, a direct Fourier-space deconvolution method may be used to reconstruct 3D index of refraction from these images in an analogous

Further author information: (Send correspondence to F.E.R)
F.E.R: E-mail: ferobles@gatech.edu
P.B.L.: E-mail: pledwig3@gatech.edu

Three-Dimensional and Multidimensional Microscopy: Image Acquisition and Processing XXVII,
edited by Thomas G. Brown, Tony Wilson, Laura Waller, Proc. of SPIE Vol. 11245, 1124503
 · doi: 10.1117/12.2544328

manner to the 2D approach, saving time and computational resources, and allowing full-field imaging and higher throughput.[7]

While both coherent and partially coherent phase contrast methods are able to produce 3D maps of refractive index from samples that are optically thick (10 μm), the need for transmissive illumination limits the available objects for imaging to transparent slices or *in-vitro* cell colonies. While label free, these other 3D QPI modalities still require substantial invasive specimen preparation, and therefore cannot compete with epi-mode label-free imaging techniques for truly non-invasive or *in-vivo* applications, despite the fact that current epi-mode label-free imaging techniques such as optical coherence tomography (OCT)[8] and confocal reflectance microscopy (CRM)[9] rely on reflected phase signals, which are weaker and less detailed due to the need for strong refractive index variations to produce back-scattering.

Recently, an illumination scheme known as oblique back-illumination (OBM) was introduced,[10] which demonstrated that phase contrast images could be produced in opaque multiply scattering samples such as whole tissue by passing light into sample from a small horizontal distance from a fiber objective. Incident light scatters multiply through the sample, illuminating the target plane from within. Due to the small offset distance, the light entering the objective has an inherent directional preference in the direction between the source and the probe, and because the light passes forward through the object plane, transmissive phase contrast is achieved.

In a previous work, we modified OBM to provide 2D quantitative phase images in epi-mode.[11] This was done by illuminating with two orthogonal pairs of horizontally-separated sources, separating the sources from the center by a larger distance to allow a high-NA microscope objective, and employing the light at a canted angle to preserve the angular preference of the scattered illumination. In order to produce an optical transfer function of the system, the trajectory of incident photons was computed using Monte Carlo simulation, and the resultant angular distribution of illuminating photons was collected and smoothed to produce the effective source distribution.

This technique, dubbed Quantitative OBM (qOBM)[12] achieves quantitative phase imaging in epi-mode in thick, opaque scattering samples, by leveraging the inherent cross sectional capabilities of an incoherent light source with a large angular extent and an objective with a relatively high NA. For biological samples such as tissue, this assumption is sufficient to accurately estimate phase in a 2D plane, but cannot produce a quantitative 3D map of index of refraction.

In this work, we outline the process of producing a 3D optical transfer function from an arbitrary source distribution, implement a 1st-Born forward model of the system, and explain the process of validating and assessing the efficacy of a direct linear reconstruction of a 10-μm bead in qOBM simulation and experiment. Finally we show Fourier-space experimental results of 3D index of refraction reconstruction in unaltered whole brain tissue *ex-vivo*.

2. METHODS

2.1 System Transfer Function - 2D

The construction of a 2D linear transfer function for a transmission microscope is well described in the literature,[13–16] and typically proceeds from a propagation of the mutual coherence in the system (or, alternately, the incoherent field) from the effective source distribution through the sample plane, then through the pupil and onto the camera. Under a paraxial assumption, the field undergoes a 2D Fourier transformation in each transition from near to far field. This operation can be summarized for a single coherent illuminating plane wave by:

$$I(\mathbf{r}) = \left|\mathcal{F}^{-1}\left\{P(\mathbf{f})\mathcal{F}\left\{o(\mathbf{x})\mathcal{F}^{-1}\left\{E(\mathbf{u})\right\}\right\}\right\}\right|^2 \tag{1}$$

where $\mathbf{u}$, $\mathbf{x}$, $\mathbf{f}$, $\mathbf{r}$ are wavelength-normalized coordinates in the source, object, pupil, and camera planes, respectively. Here P($\mathbf{f}$) is the pupil function, E($\mathbf{u}$) is an incident plane wave, and o($\mathbf{x}$) is the complex object transmission function. This function can be evaluated into a convolution of the object and its own complex conjugate with a four-dimensional transfer function scaling factor. After some variable substitutions:[12]

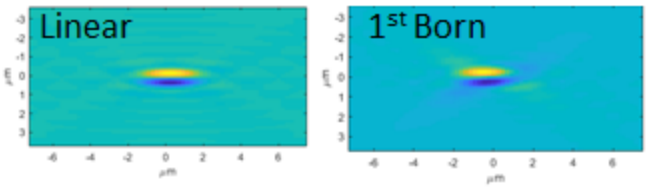

Figure 1. Y-Z cross-sections of the incoherent point-spread function of the qOBM microscope produced from the 3D linear transfer function (*left*), and from the 1st Born forward model (*right*). Visual discrepancies come from the fact that the 1st Born model incorporates dark-field terms that the linear model is obligated to exclude.

$$\tilde{I}(\mathbf{q}) = \int O(\mathbf{m})O^*(\mathbf{m}-\mathbf{q})C(\mathbf{m},\mathbf{m}-\mathbf{q})\,d^2\mathbf{m}, \tag{2}$$

where O($\mathbf{m}$) is the object transmission function in Fourier space, C($\mathbf{m}$,$\mathbf{m}-\mathbf{q}$) is the four dimensional transfer function, $\mathbf{m}$ is a shifted coordinate in the pupil space, and $\mathbf{q}$ are coordinates in the Fourier space of the camera. To make this integral manageable, a weak object assumption reduces the transfer function to two dimension, and eliminates the need for the complex conjugation of the object transmission function, so that the image formed on the camera can be expressed succinctly as $I(\mathbf{r}) = o(\mathbf{x}) * c(\mathbf{x})$ where c($\mathbf{x}$) is the point spread function (PSF) of the system. For a differential phase contrast image taken from the difference of OBM illuminations from opposite sides, normalized by their sum, the system transfer function takes the form:

$$C_{DPC}(\mathbf{q}) = \frac{-i \cdot \int \left[S(\mathbf{u}) - S(\mathbf{u}')\right] P(\mathbf{u}+\mathbf{q})P^*(\mathbf{u})\,d^2\mathbf{u}}{\int S(\mathbf{u})P(\mathbf{u})P^*(\mathbf{u})\,d^2\mathbf{u}}, \tag{3}$$

where $S(\mathbf{u})$ is the effective source intensity distribution in incident angle. This transfer function can be seen to depend on two system-dependent factors, the (exit) pupil function of the system $P(\mathbf{u})$, which for qOBM is taken as a discrete mask for angles that fall within the acceptance angle of the objective, and the effective source angular distribution $S(\mathbf{u})$. For qOBM, this latter quantity is, in general, unknown, and is found by performing a Monte Carlo photon transport simulation through a model of the tissue under investigation. Therefore once $S(\mathbf{u})$ is computed, $o(\mathbf{x})$ can be recovered quickly through direct regularized deconvolution.

2.2 Linear Transfer Function - 3D

While this reconstruction is effective for producing 2D images from differential phase contrast images from OBM, it assumes that the entire extent of the object in view exists within the focus depth of the microscope. However, with an incoherent effective illumination such as the semi-diffuse light impinging on a target in qOBM, the effective axial range is limited (see Fig. 1). This shallow focusing depth enables the effective depth cross-sectioning of OBM, but in order to quantify refractive index, this extent must be known and taken into account in the reconstruction, especially for objects that extend beyond the focusing depth of the system.

Just as a 2D system transfer function can describe a 2D transmission microscope, a 3D transfer function can be derived, beginning from the 3D Helmholz equation,[14] and proceeding from propagation of mutual intensity.[17] The phase transfer function produced in this way is given by:[17]

$$T_p(\mathbf{m},w) = \frac{\lambda}{4\pi}\int P(\mathbf{m}+\tfrac{1}{2}\mathbf{u})\Big[S(\mathbf{m}+\tfrac{1}{2}\mathbf{u}) - S(\mathbf{m}-\tfrac{1}{2}\mathbf{u})\Big]P^*(\mathbf{m}-\tfrac{1}{2}\mathbf{u})\delta(w+\lambda\mathbf{m}\cdot\mathbf{u})d^2\mathbf{u} \tag{4}$$

Analogously to the 2D case, linearizing the system behavior requires a weak object assumption, which, for the portion of the object that falls within the axial extent of the PSF of an incoherent system such as qOBM, can be true in biological samples. It should be noted from Eq. 4 that a difference of images in the illumination is not, in principle, necessary in order to acquire phase contrast from a through-stack of images, as phase information is carried through the propagation of intensity. However, as there is inherent ambiguity between phase and

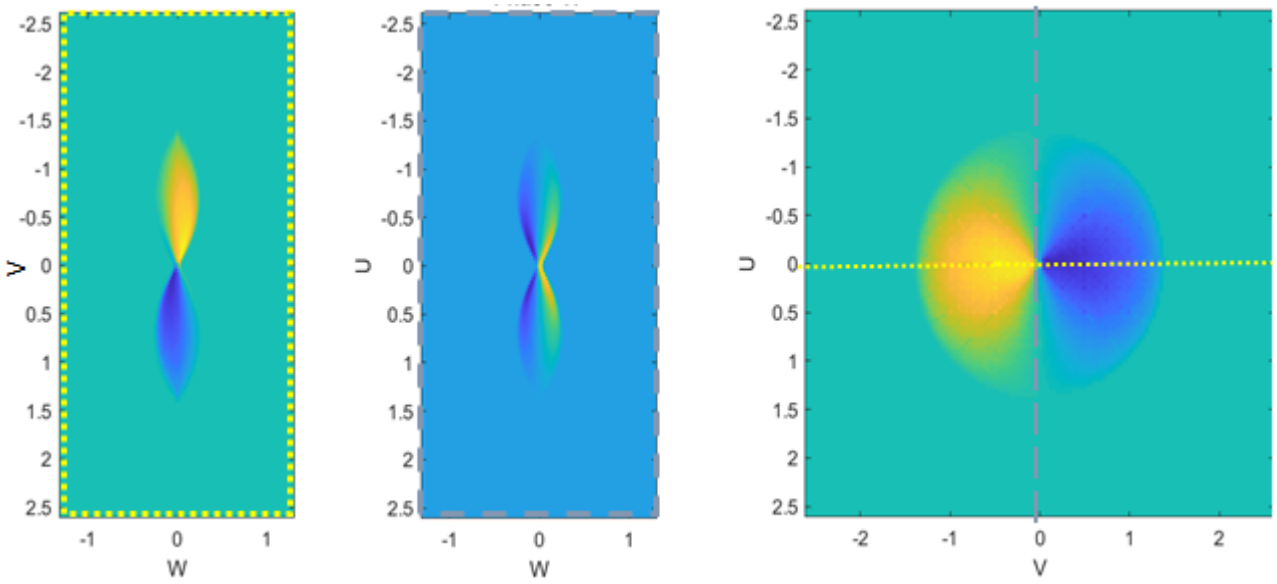

Figure 2. Cross sections through a paraxial qOBM phase transfer function for 1% intralipid agar as a scattering medium. U, V, and W represent wavelenth-normalized spatial frequencies in the x,y, and z directions, respectively. Left: cross-section in the direction between source and detector. Center: cross section perpendicular to this direction, where a typical 2D transfer function would show no phase contrast. Right: cross section in the U-V plane. The 2D transfer function is the projected sum of the 3D transfer function in this direction. Dashed and dotted lines represent the cross section locations for the figures in the center and left, respectively.

absorption due to the inadequacy of the weak object assumption for large objects, images are collected in the differential phase qOBM configuration to remove that ambiguity.

Therefore to quantify 3D refractive index, it was necessary to implement Eq. 4 numerically to produce a 3D transfer function for a given source distribution. This was accomplished by performing a convolution by looping through incident angles, and depositing the resulting sum in the z-spatial frequency position described by the delta function in Eq. 4 . A non-paraxial version was also produced in which the source function is scaled by the inverse cosine of the axial angle, and the term in the delta function was modified to describe the intersection of spherical shells rather than a plane.[18] The phase transfer function is achieved using the odd component of the source distribution, while the amplitude transfer function uses the even component. An example 3D transfer function is shown in Fig. 2. This method was validated against the analytical evaluation of Eq. 2 for a uniform illumination. Fig. 3 shows a comparison of the numerically evaluated (paraxial) phase transfer function versus the analytically evaluated one. Fringes are present in the former due the discrete nature of the convolution, such that high lateral frequency regions may receive values that are slightly skewed unless sampling in exposure angle is sufficiently high.

2.3 1st Born Forward Model

To validate the performance of the subsequent deconvolution, it would be inadequate to simulate the qOBM microscope with the linear 3D transfer function itself, as that would only test the fidelity of the reconstruction method and not its validity in a physical system. Therefore, a 1st-Born model was developed to simulate the 3D image stack formed, evaluating the equation:[19]

$$E(\mathbf{x}) \approx E_1(\mathbf{r}) \equiv e^{ik\mathbf{u}\cdot\mathbf{x}} + \int V(\mathbf{x}')e^{ik\mathbf{u}\cdot\mathbf{x}'}\frac{e^{ik|\mathbf{x}-\mathbf{x}'|}}{|\mathbf{x}-\mathbf{x}'|}d^3\mathbf{x}'. \tag{5}$$

Here E represents the scalar field, and k is the wavenumber, $2\pi/\lambda$. This model is more accurate than the linear transfer function model, as it includes the contribution of dark-field illumination—source angles that fall

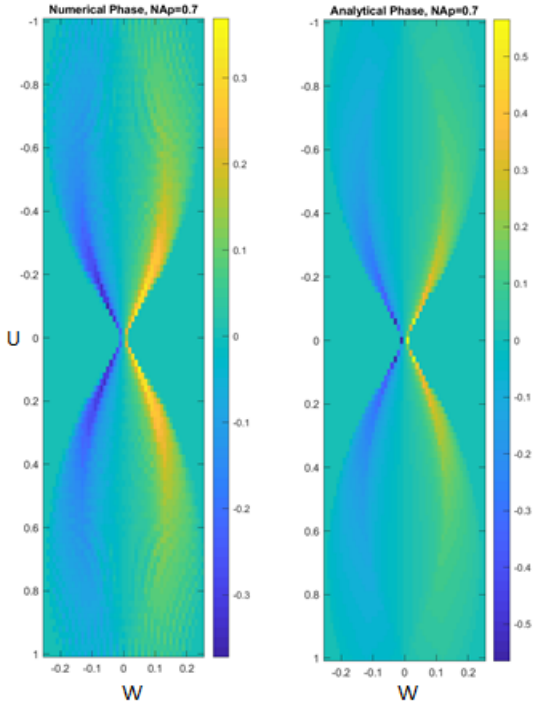

Figure 3. U-W cross sections in the 3D phase transfer function produced numerically (*left*) and analytically (*right*). The axis label U represents the wavelength-normalized spatial frequency in the x-direction, and W represents the same for the z-direction.

outside of the objective pupil. However, it is based on the 1st Born approximation that assumes that the detected field comes from the first scattering interaction between the object and the incident field, equivalent to a single scattering event. For a coherent source, this assumption could be inadequate for thick, highly scattering objects, but for an incoherent source such as that produced by qOBM, the limited axial extent of the transfer function means that higher order scattering withing the limit of the PSF is unlikely in biological samples. Multiple diffuse scattering in qOBM, therefore, manifests as reduction in SNR as the plane of focus is moved deeper into the sample, as incoherent out-of-plane contributions from higher-order scattering reduce the visibility of phase features in the field of view.

2.4 Polystyrene Bead Validation

To validate the 3D transfer function direct deconvolution in experiment, we compared reconstruction results of a 10-μm polystyrene bead (n=1.59) embedded in a thermoplastic of known refractive index (Cargille, n=1.53), beneath an 1% intralipid-agar tissue phantom with known scattering properties. Through-stack images were taken in experiment (Δz=.5μm), and analogous data was produced in simulation. Two methods of reconstruction were then performed. In the first, the data was treated as an independent series of 2D phase contrast images, and each was reconstructed according to the 2D transfer function, and an estimate of refractive index was produced by solving the optical path length formula for index of refraction n(x):

$$\Delta\phi = \frac{\lambda}{2\pi}\Delta z\big(n(\mathbf{x}) - n_0\big). \tag{6}$$

Here λ is the wavelength, ϕ is the phase value produced from the 2D deconvolution, and n_0 is the background index of refraction. The second method involved performing regularized 3D direct deconvolution of the entire through stack of images, using the synthesized 3D transfer function. For this method, index of refraction was computed by solving the scattering potential formula for index of refraction:

$$V(\mathbf{x}) = \left(\frac{2\pi}{\lambda}\right)^2 \left(n(\mathbf{x})^2 - n_0^2\right). \tag{7}$$

The reason for this discrepancy is that the 2D and 3D transfer functions have different starting points in their derivations, the former starting from angular spectrum decomposition of a thin 2D object and the latter starting from the Helmholtz scalar partial differential equation with a scalar potential giving rise to the scattering.

Finally, to obtain a biological demonstration of this principle, an otherwise unaltered rat brain was coronally sectioned in half, and placed section-down on a glass slide to be imaged by qOBM. Through-stack images were taken on the edge of a lateral ventricle with choroid plexus, the tissue that produces cerebrospinal fluid in the brain.[20] This tissue contains the microscopic structure of epithelial secretory cells, as well as mesoscopic folds that protrude and allow for multi-scale evaluation of our 3D reconstruction technique.

3. RESULTS

The stacked 2D reconstruction of index of refraction fails to take into account the axial extent of the PSF of the system, leading to an underestimation for thick objects. An explanation of this can be seen by examining the Fourier space of the reconstructed object in each case, as depicted in Fig. 4. By treating each slice as its own 2D transmission object, the support structure of the reconstructed object (Fig 4 *bottom*) maintains constant intensity in the z-spatial frequency. This amplifies high-frequency noise that does not contain structural information passed through the microscope and acts as a high-pass filter on image features that are low-frequency in z, hollowing out large-scale features. The 3D reconstruction, by contrast (Fig. 4 *top*), effectively reconstructs low-frequency features in z and cuts out noise information that is not present in the object's transmission through the image.

4. CONCLUSION

While the depth-sectioning inherent to highly incoherent transmission microscopy enables tomographic reconstruction from a through-stack of individually reconstructed 2D phase images, information about the path over which this phase is integrated is lost with this method, and the resulting image can not be said to reproduce the index of refraction of a sample. In order to address this, a 3D transfer function deconvolution approach was taken to reconstruct a 3D map of index of refraction from a through stack of qOBM images, allowing for quantitative 3D refractive index imaging in unaltered thick, opaque, multiply scattering samples. These methods open the door for further quantitative analysis of systems with arbitrary source distributions and the results establish qOBM as the only epi-mode imaging technique capable of producing quantitative 3D maps of refractive index in unaltered whole tissue.

ACKNOWLEDGMENTS

This work was funded by the Burroughs Welcome Fund (BWF) (1014540); Marcus Center for Therapeutic Cell Characterization and Manufacturing (MC3M); National Cancer Institute (NCI) (R21CA223853); National Science Foundation (NSF CBET CAREER 1752011), and Georgia Institute of Technology.

REFERENCES

[1] Park, J. H., Yu, Z., Lee, K. R., Lai, P., and Park, Y. K., "Perspective: Wavefront shaping techniques for controlling multiple light scattering in biological tissues: Toward in vivo applications," *APL Photonics* **3** (oct 2018).

[2] Sheppard, C. and Wilson, T., "Image Formation in Scanning Microscopes with Partially Coherent Source and Detector," *Optica Acta: International Journal of Optics* **25**, 315–325 (apr 1978).

[3] Mehta, S. B. and Sheppard, C. J. R., "Partially coherent image formation in differential interference contrast (DIC) microscope," *Optics Express* **16**, 19462 (nov 2008).

[4] Tian, L. and Waller, L., "3D intensity and phase imaging from light field measurements in an LED array microscope," *Optica* **2**, 104 (feb 2015).

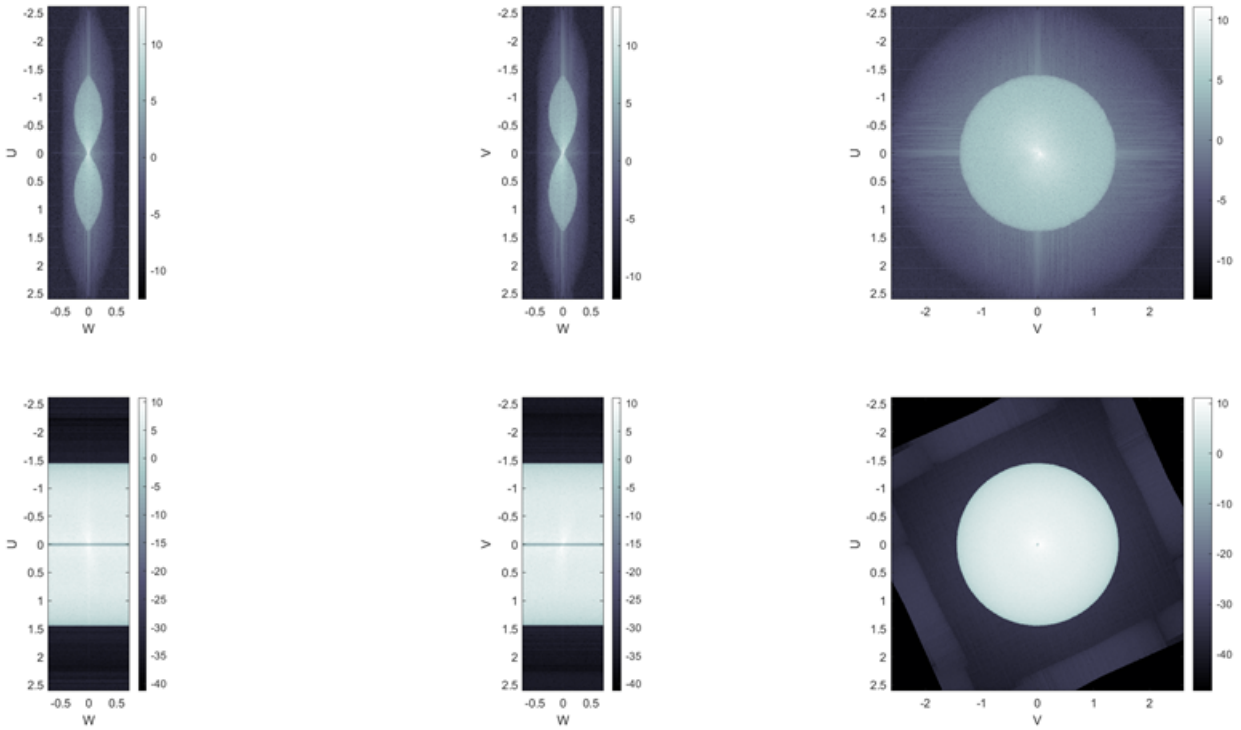

Figure 4. Log-amplitude cross sections in the Fourier space of reconstructed images from unaltered choroid plexus. *Top Left, Center, Right*: cross sections through the V-W, U-W, and U-V planes respectively of the object reconstructed with the 3D refractive index reconstruction method. *Bottom Left, Center, Right*: cross sections through the V-W, U-W, and U-V planes respectively of the object reconstructed with the 2D quantitative phase image stacking method.

[5] Choi, W., Fang-Yen, C., Badizadegan, K., Oh, S., Lue, N., Dasari, R. R., and Feld, M. S., "Tomographic phase microscopy," *Nature methods* **4**(9), 717–719 (2007).

[6] Jin, D., Zhou, R., Yaqoob, Z., and So, P. T. C., "Tomographic phase microscopy: principles and applications in bioimaging [Invited]," *Journal of the Optical Society of America B* **34**, B64 (may 2017).

[7] Chen, M., Tian, L., and Waller, L., "3D differential phase contrast microscopy," *Biomedical Optics Express* **7**, 3940 (oct 2016).

[8] Huang, D., Swanson, E. A., Lin, C. P., Schuman, J. S., Stinson, W. G., Chang, W., Hee, M. R., Flotte, T., Gregory, K., and Puliafito, C. A., "Optical coherence tomography.," *Science (New York, N.Y.)* **254**, 1178–81 (nov 1991).

[9] White, W. M., Rajadhyaksha, M., González, S., Fabian, R. L., and Anderson, R. R., "Noninvasive Imaging of Human Oral Mucosa in Vivo by Confocal Reflectance Microscopy," *The Laryngoscope* **109**, 1709–1717 (oct 1999).

[10] Ford, T. N., Chu, K. K., and Mertz, J., "Phase-gradient microscopy in thick tissue with oblique back-illumination," *Nature Methods* **9**, 1195–1197 (dec 2012).

[11] Ledwig, P., Sghayyer, M., Kurtzberg, J., and Robles, F. E., "Dual-wavelength oblique back-illumination microscopy for the non-invasive imaging and quantification of blood in collection and storage bags," *Biomedical Optics Express* **9**, 2743 (jun 2018).

[12] Ledwig, P. and Robles, F. E., "Epi-mode tomographic quantitative phase imaging in thick scattering samples," *Biomedical optics express* **10**(7), 3605–3621 (2019).

[13] Hopkins, H. H., "On the Diffraction Theory of Optical Images," *Proceedings of the Royal Society A: Mathematical, Physical and Engineering Sciences* **217**, 408–432 (may 1953).

[14] Born, M. and Wolf, E., [*Principles of optics : electromagnetic theory of propagation, interference and diffraction of light*], Cambridge University Press (1999).
[15] Goodman, J. W., [*Introduction to Fourier optics*], Roberts & Co (2005).
[16] "The frequency response of a defocused optical system," *Proceedings of the Royal Society of London. Series A. Mathematical and Physical Sciences* **231**, 91–103 (jul 1955).
[17] Streibl, N., "Three-dimensional imaging by a microscope," *Journal of the Optical Society of America A* **2**, 121 (feb 1985).
[18] Bao, Y. and Gaylord, T. K., "Quantitative phase imaging method based on an analytical nonparaxial partially coherent phase optical transfer function," *Journal of the Optical Society of America A* **33**, 2125 (nov 2016).
[19] Born, M., Wolf, E., Bhatia, A. B., Clemmow, P. C., Gabor, D., Stokes, A. R., Taylor, A. M., Wayman, P. A., and Wilcock, W. L., [*Principles of Optics*], Cambridge University Press, Cambridge (1999).
[20] Guyton, A. C., Hall, J. E., et al., [*Textbook of medical physiology*], vol. 548, Saunders Philadelphia (1986).